A: Environmental, Combustion, and Atmospheric Chemistry; Aerosol Processes, Geochemistry, and Astrochemistry

# Temperature Dependence of the Reaction of Chlorine Atoms with CHOH and CHCHO

Aileen O. Hui, Mitchio Okumura, and Stanley P Sander

*J. Phys. Chem. A*, **Just Accepted Manuscript** • DOI: 10.1021/acs.jpca.9b00038 • Publication Date (Web): 15 May 2019

# Temperature Dependence of the Reaction of Chlorine Atoms with $CH_3OH$ and $CH_3CHO$

Aileen O. Hui,*,† Mitchio Okumura,*,† and Stanley P. Sander*,‡

†*Arthur Amos Noyes Laboratory of Chemical Physics, Division of Chemistry and Chemical Physics, California Institute of Technology, M/S 127-72, 1200 East California Boulevard, Pasadena, California 91125*

‡*Jet Propulsion Laboratory, California Institute of Technology, 4800 Oak Grove Drive, Pasadena, California 91109*

E-mail: aileenh@caltech.edu; mo@caltech.edu; stanley.p.sander@jpl.nasa.gov

**Abstract**

Rate constants of the reactions Cl + $CH_3OH \longrightarrow CH_2OH$ + HCl ($k_1$) and Cl + $CH_3CHO \longrightarrow CH_3C(O)$ + HCl ($k_3$) were measured at 100 Torr over the temperature range 230.3 - 297.1 K. Radical chemistry was initiated by pulsed laser photolysis of $Cl_2$ in mixtures of $CH_3OH$ and $CH_3CHO$ in a flow reactor. Heterodyne near-IR (NIR) wavelength modulation spectroscopy was used to directly detect $HO_2$ produced from the subsequent reaction of $CH_2OH$ with $O_2$ in real-time to determine the rate of reaction of Cl with $CH_3OH$. The rate of Cl + $CH_3CHO$ was measured relative to that of the Cl + $CH_3OH$ reaction. Secondary chemistry, including that of the adducts $HO_2 \cdot CH_3OH$ and $HO_2 \cdot CH_3CHO$, were taken into account. The Arrhenius expressions were found to be $k_1(T) = 5.02^{+1.8}_{-1.5} \times 10^{-11} \exp[(20 \pm 88)/T]$ cm$^3$ molecule$^{-1}$ s$^{-1}$ and $k_3(T) = 6.38^{+2.4}_{-2.0} \times 10^{-11} \exp[(56 \pm 90)/T]$ cm$^3$ molecule$^{-1}$ s$^{-1}$ ($2\sigma$ uncertainties). The average values of the rate constants over this temperature range were $k_1 = (5.45 \pm 0.37) \times 10^{-11}$ cm$^3$ molecule$^{-1}$ s$^{-1}$ and $k_3 = (8.00 \pm 1.27) \times 10^{-11}$ cm$^3$ molecule$^{-1}$ s$^{-1}$ ($2\sigma$ uncertainties), consistent with current literature values.

# Introduction

Organic free radicals are ubiquitous intermediates in the Earth's troposphere, formed from the oxidation of volatile organic compounds (VOCs). Due to their key roles in air quality, oxidation reactions forming free radicals are of great interest in atmospheric chemistry. While OH is the primary daytime oxidant, Cl atoms can be the major oxidant locally in certain regions, such as in the marine boundary layer.[1–3] Furthermore, Cl atoms may be more ubiquitous than previously assumed;[4–9] Raff et al.[10] have recently proposed that Cl atoms may be generated from the photolysis of $ClNO_2$ formed by heterogeneous reactions.

$CH_3OH$ and $CH_3CHO$ are two major components of oxygenated volatile organic compounds (OVOC) in the troposphere. They are biogeochemically active and serve as tracers of biogenic emission. $CH_3OH$ is present throughout the atmosphere and is

the second most abundant VOC after $CH_4$.[11] $CH_3CHO$ is a primary pollutant produced from ethanol combustion, and is also formed from the photoxidation of VOCs.[12–14] In the atmosphere, their reactions with Cl atoms are followed rapidly by reaction with $O_2$ to form peroxy radicals ($HO_2$ and $CH_3C(O)O_2$, respectively):

$$Cl + CH_3OH \longrightarrow CH_2OH + HCl \quad \text{(R1)}$$
$$CH_2OH + O_2 \longrightarrow HO_2 + CH_2O \quad \text{(R2)}$$

$$Cl + CH_3CHO \longrightarrow CH_3C(O) + HCl \quad \text{(R3)}$$
$$CH_3C(O) + O_2 \xrightarrow{M} CH_3C(O)O_2 \quad \text{(R4)}$$

Accurate characterization of the rate constants, $k_1$ and $k_3$, over an atmospherically-relevant range of temperatures is thus important in modeling $CH_3OH$ and $CH_3CHO$ chemistry in regions of the troposphere where Cl-atom oxidation dominates. In the laboratory, Cl atoms are commonly used to generate free radicals. The reactions of Cl atoms with $CH_3OH$ (R1) and $CH_3CHO$ (R3) have been widely used to source hydroperoxy ($HO_2$) and acetylperoxy ($CH_3C(O)O_2$) radicals, respectively. Both reactions have been used simultaneously in studies of the kinetics and product yields of the $HO_2 + CH_3C(O)O_2$ cross-reaction.[15–24] The accuracy in the experimentally-determined kinetics parameters of reactions such as $HO_2 + CH_3C(O)O_2$ are limited in part by the uncertainties in $k_1$ and $k_3$.

Numerous room temperature studies have investigated the rate constants of R1[25–32] and R3[26,29–31,33–37] using relative and absolute rate methods, with consistent results in the reported values of $k_1$ and $k_3$. However, the temperature dependences of R1 and R3 are not as well-defined. Although the temperature dependence of $k_1$ has been extensively studied,[38–41] there are disagreements among the different studies. The direct study by Michael et al.[38] reported R1 to be temperature-independent over the temperature range $T$ = 200 - 500 K, and was consistent with the indirect study by Lightfoot et al.[39] ($T$ = 248 - 573 K). On the other hand, the work by Garzón et al.[40] suggested that R1 has a significant

temperature dependence over the range $T$ = 266 - 380 K. Kaiser and Wallington[41] also reported a weaker temperature dependence over the range $T$ = 291 - 475 K using relative rate measurements. The JPL data evaluation has not recently reevaluated R1, and is current only up to the JPL02-25 recommendation in 2003.[42] Thus, the JPL evaluation does not include the more recent works by Garzón et al.[40] and Kaiser and Wallington[41], and recommends R1 to be temperature-independent.[42] The IUPAC evaluation suggests that Garzón et al.[40] may have overestimated the activation barrier and also excludes the results from Garzón et al.[40] in their recommendations;[43] however, a small temperature dependence for R1 is recommended based on the work by Kaiser and Wallington[41].

The temperature dependence of $k_3$ is also not well-characterized. The temperature dependence of $k_3$ has only been investigated once by Payne et al.[44], whose results showed that $k_3$ was temperature-independent over the range $T$ = 210 - 343 K. Their measured value of $k_3 = (6.6 \pm 1.4) \times 10^{-11}$ cm$^3$ molecule$^{-1}$ s$^{-1}$ was on the lower range of the values reported by other previous measurements at room temperature, albeit still within the uncertainty limits. The IUPAC data evaluation recommends $k_3$ to be temperature-independent based on the single study, and there is currently no recommendation for R1 in the JPL evaluation.

The diverse experimental techniques used in previous measurements of $k_1$ and $k_3$ include both absolute and relative rate methods. A majority of the previous studies obtained kinetics data by directly or indirectly monitoring the rate of disappearance of the reactants (i.e., $CH_3OH$,[26,27,29,41] $CH_3CHO$,[26,29,33–35] or Cl atoms[25,28,29,32,38,40,44]). The accuracy of the rate constants determined from relative rate methods are generally limited by the reference reaction, as well as by other reactions that competitively remove the measured reagents (i.e., $CH_3OH$ and/or $CH_3CHO$). Resonance fluorescence techniques offer high sensitivity to Cl atoms but require proper characterization of additional losses such as wall reactions, quenching, and diffusion.

A few studies have used product detection to determine the rate constants (e.g. HCl

product from R1[30,31] and R3[30,31,36]), but were only carried out at room temperature. A recent work by Howes et al.[37] demonstrated that accurate measurement of $k_3$ could be obtained by monitoring the $CH_3C(O)$ product using photo-ionization mass spectrometry. A value of $k_3 = (7.7 \pm 0.7) \times 10^{-11}$ cm$^3$ molecule$^{-1}$ s$^{-1}$ at room temperature was reported, in excellent agreement with the IUPAC recommendations.

In this work, we measured $k_1$ and $k_3$ by detecting the $HO_2$ product formed via R2. Cl atoms were generated using pulsed laser photolysis and $HO_2$ was monitored in the near-IR (NIR) in real-time using IR $2f$ wavelength modulation spectroscopy (WMS). The main advantage of our technique was our high sensitivity to $HO_2$ radicals and a well-defined overlap between the photolysis volume and the detected radical product. The temperature dependences of $k_1$ and $k_3$ were determined over the temperature range 230.3 - 297.1 K at 100 Torr in $N_2$. Gas mixtures containing $Cl_2/O_2/N_2/CH_3OH$ or $Cl_2/O_2/N_2/CH_3CHO$ were used to determine $k_1$ and $k_3$, respectively, using pseudo-first order kinetics. All experiments were carried out under conditions where the $O_2$, $CH_3OH$, and $CH_3CHO$ concentrations were all in excess relative to Cl atoms.

# Experimental Methods

The Infrared Kinetics Spectroscopy (IRKS) apparatus consisted of a temperature-controlled pulsed laser photolysis flow cell coupled to simultaneous IR and UV absorption spectroscopy and has been described in detail previously.[45–47] Only the details pertinent to the present work will be provided, including modifications that were made since the last publication.

The flow cell was a jacketed Pyrex cell of length 175 cm and diameter 5 cm and was temperature-controlled by flowing liquid nitrogen-cooled methanol circulating through the jacket of the cell. The temperature was measured with a calibrated type T thermocouple (Omega) inserted into the jacket of the cell. This temperature measurement was consistent

with in-situ measurements made inside of the cell. The temperature profile along the length of the cell was verified to be uniform across the volume probed by the IR laser. Reagent gases were pre-mixed and pre-cooled in a Pyrex manifold prior to entering the cell. Room temperature $N_2$ purge gas flowed from the aluminum chambers on either end of the cell towards the gas pump-out ports to confine the main gas flow to the temperature controlled region and to protect the Herriott mirrors that formed the multi-pass optical cavity for the IR probes. The gas flows were regulated by mass flow controllers (MKS Instruments) and the total flow rate was kept at approximately 2000 $cm^3$ (STP) $min^{-1}$, maintaining a 10 s residence time inside the flow cell at a total pressure of $100 \pm 2$ Torr. $CH_3OH$ and $CH_3CHO$ were introduced into the cell by flowing $N_2$ through glass bubblers containing the liquid compounds, held inside temperature-controlled baths. The pressures in the reaction cell and bubblers were measured by absolute capacitance pressure gauges (MKS Baratron), and the concentrations of $CH_3OH$ and $CH_3CHO$ vapors were determined from their flow rates using the known vapor pressures of the pure compounds and assuming complete saturation in the bubblers.

351 nm light from a XeF excimer laser (Compex 301) operating in the constant energy mode was directed coaxially through the flow cell to initiate the chemistry by photolyzing $Cl_2$ molecules in gas mixtures of $Cl_2/N_2/O_2/CH_3OH/CH_3CHO$. A photolysis repetition rate of 0.2 Hz was used, resulting in two photolysis events occurring per residence time. Decreasing the repetition rate to 0.1 Hz made no difference in the kinetics traces. At repetition rates above 0.2 Hz we observed small changes in the kinetics traces due to possible photolysis of reaction products. For this reason, the repetition rates were limited to 0.2 Hz and below.

All experiments were conducted using excess concentrations of $O_2$, $CH_3OH$, and $CH_3CHO$ relative to the initial radical concentrations, such that all Cl atoms generated from photolysis were assumed to form either $HO_2$ or $CH_3C(O)O_2$ via R1 and R3, respectively. Typical concentrations of the reagents were: $[CH_3OH] = (2.4 - 10.7) \times 10^{15}$ molecules

$cm^{-3}$, $[CH_3CHO] = (0.9 - 8.4) \times 10^{15}$ molecules $cm^{-3}$, $[O_2] = (1.6 - 2.0) \times 10^{18}$ molecules $cm^{-3}$; $[Cl_2] = (0.8 - 5.3) \times 10^{15}$ molecules $cm^{-3}$, with total radical concentrations of $[Cl]_0 = (1.8 - 19) \times 10^{13}$ molecules $cm^{-3}$.

A 3 mW continuous-wave (CW) distributed feedback (DFB) laser operating in the NIR was used for sensitive detection of $HO_2$ radicals. The diode laser was tuned to the rovibrational transitions of the first overtone of the OH stretch of $HO_2$ ($2\nu_1$: 6638.2 $cm^{-1}$). The laser output was wavelength modulated at 6.8 MHz by sinusoidally modulating the injection current with an external function generator. 2f-heterodyne detection was implemented by demodulating the detected signal at 13.6 MHz. The demodulated signal was collected at a sampling rate of 2.5 MHz, amplified by a factor of 200, and low-pass filtered at 1 MHz using a low-noise preamplifier (SRS SR560). The noise-equivalent concentration per $Hz^{-1/2}$ of $HO_2$ normalized to one excimer shot was $2.9 \times 10^9$ molecules $cm^{-3}$ $Hz^{-1/2}$. For a typical experimental run, the $HO_2$ signal was averaged for 65 - 75 excimer laser shots and the minimum detectable concentration of $HO_2$ was $\sim 4 \times 10^{10}$ molecules $cm^{-3}$. Although we had the sensitivity to perform the experiment at lower overall radical concentrations, the higher concentration provided better signal-to-noise ratios and under our conditions, did not further complicate the kinetics.

Since WMS only measures the relative changes in concentration, the $HO_2$ laser was calibrated daily to obtain absolute concentrations. The $HO_2$ laser was calibrated against UV absorption at $\lambda$= 225 nm ($\sigma_{HO_2} = 2.88 \times 10^{-18}$ $cm^2$ $molecule^{-1}$) by measuring the NIR and UV decay signals simultaneously when $HO_2$ was the only peroxy radical present; i.e., $[CH_3CHO] = 0$. This calibration procedure has been used previously and is described in more detail elsewhere.[15] A thorough discussion and comparison of other $HO_2$ calibration methods can also be found in Onel et al.[48] Broadband UV light was provided by a laser-driven light source (Energetiq EQ-99XFC). The collimated UV beam was coaligned with and counter-propagated the excimer beam, making a single pass through the cell. A monochromator (Acton Research Corporation Spectra Pro-300i) placed in front of a

photomultiplier tube (PMT) was used for wavelength-specific detection of the transmitted UV light. Baffles were placed on both ends of the flow cell to ensure that only light that sampled the photolysis volume entered the monochromator. Despite a different geometric overlap due to the off-axis orientation of the Herriott mirrors, the IR and UV probe beams should capture the same physical processes at relatively short timescales ($< 20$ ms); i.e., before diffusion becomes a significant loss process. At the beginning of every experiment, the kinetics traces from the $HO_2$ self-reaction were collected at three different initial radical concentrations at room temperature. The IR and UV traces were simultaneously fit to a bimolecular decay using the kinetics modeling program, FACSIMILE,[49] to obtain the calibration factor, which converts the IR signal in mV to the absolute $HO_2$ concentration.

# Results and Discussion

All experiments were conducted using excess concentrations of $O_2$, $CH_3OH$, and $CH_3CHO$ relative to the total initial radical concentration, $[Cl]_0$. $[O_2]$ was in excess of [Cl] by at least a factor of $10^4$, and $[CH_3OH]$ and $[CH_3CHO]$ were typically in excess of [Cl] by at least a factor of 20. Kinetics modeling showed that the ratios of [Cl] to $[O_2]$, $[CH_3OH]$, and $[CH_3CHO]$ under these conditions had no effect on the returned values of $k_1$ and $k_3$. $[O_2]$ was also in excess of both $[CH_3OH]$ and $[CH_3CHO]$, such that the first order loss rates of R4 and R2 were at least 10 times greater than both R1 and R3. For example, at the lowest $O_2$ concentration ($[O_2]$=$1.6 \times 10^{18}$ molecules cm$^{-3}$) and highest $CH_3OH$ and $CH_3CHO$ concentrations ($\sim 1 \times 10^{16}$ molecules cm$^{-3}$), the first order loss rates were

$$k_2[O_2] \sim 8 \times 10^6 \text{ s}^{-1} \quad \approx 15k_1[CH_3OH] \approx 14k_3[CH_3CHO] \quad (1)$$

$$k_4[O_2] \sim 1 \times 10^8 \text{ s}^{-1} \quad \approx 160k_1[CH_3OH] \approx 150k_3[CH_3CHO] \quad (2)$$

where

$$k_2 \sim 9.1 \times 10^{-11}\ \text{cm}^3\ \text{molecule}^{-1}\ \text{s}^{-1} \quad \text{(ref: JPL 15-10}^{42}\text{)} \quad (3)$$

$$k_4 \sim 5.1 \times 10^{-12}\ \text{cm}^3\ \text{molecule}^{-1}\ \text{s}^{-1} \quad \text{(ref: Atkinson et al.}^{50}\text{)} \quad (4)$$

$$k_1 \sim 5.5 \times 10^{-11}\ \text{cm}^3\ \text{molecule}^{-1}\ \text{s}^{-1} \quad \text{(ref: JPL 15-10}^{42}\text{)} \quad (5)$$

$$k_3 \sim 8.0 \times 10^{-11}\ \text{cm}^3\ \text{molecule}^{-1}\ \text{s}^{-1} \quad \text{(ref: IUPAC}^{43}\text{)} \quad (6)$$

Thus, the rate-limiting steps for the formation of $HO_2$ and $CH_3C(O)O_2$ can be approximated to be R1 and R3, respectively; i.e.,

$$Cl + CH_3OH \longrightarrow HO_2 \quad (R5)$$

$$Cl + CH_3CHO \longrightarrow CH_3C(O)O_2 \quad (R6)$$

The formation of $HO_2$ and $CH_3C(O)O_2$ were pseudo-first order since both $[CH_3OH]$ and $[CH_3CHO]$ were in excess relative to $[Cl]_0$; therefore, the rate law for $HO_2$ can be written as

$$\frac{d[HO_2]}{dt} = k_1[CH_3OH][Cl]_0 \exp[-(k_1[CH_3OH] + k_3[CH_3CHO])t] \quad (7)$$

$$= k_1'[Cl]_0 \exp[-(k_1' + k_3')t], \quad (8)$$

where $k_1'$ and $k_3'$ are the pseudo-first order rate constants for R1 and R3, respectively; i.e.,

$$k_1' = k_1[CH_3OH] \quad (9)$$

and

$$k_3' = k_3[CH_3CHO] \quad (10)$$

Experimental conditions were chosen to minimize subsequent losses of $HO_2$ via the self reaction (R7) and reaction with $CH_3C(O)O_2$ (R8).

$$HO_2 + HO_2 \xrightarrow{M} H_2O_2 + O_2 \quad (R7)$$

$$HO_2 + CH_3C(O)O_2 \longrightarrow \text{products} \quad (R8)$$

This was achieved by using sufficiently low initial radical concentrations such that the decrease in the $HO_2$ signal from ~20 - 30 $\mu$s (i.e., after conversion of Cl to $HO_2$ and

$CH_3C(O)O_2$ was completed) to ~50 $\mu$s was less than 5%.

At low temperatures, the range of experimental conditions that could be explored were additionally limited by the need to minimize the rapid loss of $HO_2$ by reaction with $CH_3OH$ and/or with $CH_3CHO$ via R9 and R10, respectively, such that Equation 8 was still valid.

$$HO_2 + CH_3OH \underset{M}{\overset{M}{\rightleftharpoons}} HO_2 \cdot CH_3OH \quad \text{(R9)}$$

$$HO_2 + CH_3CHO \underset{M}{\overset{M}{\rightleftharpoons}} HO_2 \cdot CH_3CHO \quad \text{(R10)}$$

The formation of the hydrogen-bonded adducts via R9 and R10 becomes more favored at lower temperatures. Previous studies have also shown that these adducts introduce additional loss processes for $HO_2$ via R11 and R12, resulting in an enhanced observed $HO_2$ decay rate that becomes more significant at lower temperatures, even at relatively low $CH_3OH$ and $CH_3CHO$ concentrations.[51]

$$HO_2 + HO_2 \cdot CH_3OH \longrightarrow \text{products} \quad \text{(R11)}$$

$$HO_2 + HO_2 \cdot CH_3CHO \longrightarrow \text{products} \quad \text{(R12)}$$

Therefore, $[CH_3OH]$ and $[CH_3CHO]$ were typically limited to less than $\sim 1 \times 10^{16}$ molecules $cm^{-3}$ and $\sim 5 \times 10^{15}$ molecules $cm^{-3}$, respectively, for temperatures below $T$ = 250 K in order to minimize the adduct formation and rapid loss of $HO_2$. Using the previously determined equilibrium constants for R9 and R10,[52] the upper limit of the uncertainty in the $HO_2$ concentration, calculated from the highest $[CH_3OH]$ and $[CH_3CHO]$ used, was ~2% at $T$ = 297.1 K and ~20% at $T$ = 230.3 K.

## Rate constant of Cl + $CH_3OH$ ($k_1$)

R1 was investigated by measuring the formation signal of $HO_2$ in the absence of $CH_3CHO$ at various concentrations of $CH_3OH$. In the absence of $CH_3CHO$, the integrated rate law

for $HO_2$ is given by Equation 11:

$$[HO_2] = [Cl]_0 - [Cl]_0 e^{-k_1' t} \quad (11)$$

The data were fit with a single exponential function with an effective rate constant, $k_1'$, as given by Equation 9. The data were fit starting from $t \sim 1.6$ $\mu$s to $t \sim 50$ $\mu$s. The data points for $t < 1.6$ $\mu$s were susceptible to electrical pick-up from the excimer pulse and were thus excluded from the fit. The fitted curves extrapolated to $t = 0$ showed that the data curves were well-defined by Equation 11.

The $HO_2$ formation curves measured at $T = 297.1$ K and at $T = 230.3$ K using varying $[CH_3OH]$ are shown in Figure 1(a) and Figure 1(b), respectively. The fits to the data are shown in solid lines, and the extrapolations to $t = 0$ are represented by dashed lines. Both figures demonstrate that the $HO_2$ formation rate increases with increasing $[CH_3OH]$, as expected. The observed $[HO_2]$ from the lowest $[CH_3OH]$ (blue markers) in Figure 1(b) is approximately 5% higher than the $[Cl]_0$; however, this is within the 10% uncertainty in the calibration of the NIR signal. Details on the error analysis of our calibration methods can be found elsewhere.[15] Briefly, the systematic error in the NIR calibration was determined by running Monte Carlo simulations of the simultaneous IR and UV fits. These calculations accounted for uncertainties in the UV absorption cross-sections of $HO_2$, $H_2O_2$, $k_7$, and the unimolecular diffusion rate constants.

Figure 1(a) shows that at room temperature, the $HO_2$ signals level off to a common value by $\sim 50$ $\mu$s, indicating complete conversion of Cl to $HO_2$ without significant subsequent loss of $HO_2$ via reaction with $[CH_3OH]$ (R9). On the other hand, the $HO_2$ signals in Figure 1(b) do not level off to the same value; rather, the yields of $HO_2$ appear to decrease with increasing $[CH_3OH]$. The negative dependence of the $HO_2$ yield on $[CH_3OH]$ is attributed to the rapid loss of $HO_2$ from the formation of the hydrogen-bonded adduct with $CH_3OH$ (R9). This effect was evident at temperatures below 250 K for $[CH_3OH] > 1 \times 10^{16}$ molecules $cm^{-3}$, which was used as the upper limit of the range of $[CH_3OH]$ that was

used so that Equation 11 was still valid. $[Cl]_0$ was also kept below $1 \times 10^{14}$ molecules $cm^{-3}$ for $T < 250$ K to decrease the $HO_2$ loss rate; at $T$ = 230.3 K, however, rapid loss of $HO_2$ could not completely be avoided even at the lowest $[Cl]_0$ and $[CH_3OH]$ conditions. Based on the equilibrium constant of R9 determined previously,[52] approximately 15% of $HO_2$ is predicted to be complexed at the highest $[CH_3OH] = 8.5 \times 10^{15}$ molecules $cm^{-3}$. For data collected at lower temperatures and at high $[CH_3OH]$, the number of data points in the kinetics traces that were used in the fits were reduced to minimize capturing the fast $HO_2$ loss via R9. The additional error introduced by reducing the sample size effectively accounted for the uncertainties in the fitted $[HO_2]$ assuming no subsequent loss. A subset of the data were also analyzed using methods that took into account the subsequent $HO_2$ removal via either pseudo-first order or second-order loss processes (Supporting Information). The fitted values of the rate constants in both cases were consistent with the results obtained using the simplified pseudo-first order growth model described here.

The measured values of $k_1'$ at each temperature were plotted against $[CH_3OH]$ and total linear least-squares regressions to the data were used to determine $k_1$. The pseudo-first order plots of R1 at three temperatures are shown in Figure 2. The fitted values of $k_1$ are tabulated in Table 1 along with the range of experimental conditions that were used to measure $k_1'$. The uncertainties in $k_1$ ($2\sigma$) include the random errors in $k_1'$ (typical: ~1 - 2%, maximum: ~10%) as well as systematic errors in the pressures, flows, and temperatures (total uncertainty in $[CH_3OH]$: ~2.5%).

**Table 1: Experimental conditions for determination of $k_1$. Uncertainties in $k_1$ are $2\sigma$.**

| T (K) | $[O_2]$ ($\times 10^{18}$ $cm^{-3}$) | $[Cl_2]$ ($\times 10^{15}$ $cm^{-3}$) | $[CH_3OH]$ ($\times 10^{15}$ $cm^{-3}$) | $[Cl]_0$ ($\times 10^{13}$ $cm^{-3}$) | $k_1$ ($\times 10^{-11}$ $cm^3$ $s^{-1}$) |
|---|---|---|---|---|---|
| 297.1 | 1.58 | 5.29 | 2.99 - 8.84 | 19 | $5.58 \pm 0.36$ |
| 294.8 | 1.58 | 1.49 | 2.60 - 7.49 | 4.6 | $5.53 \pm 0.42$ |
| 280.2 | 1.66 | 1.56 - 3.8 | 2.98 - 8.01 | 5.1 - 13 | $5.21 \pm 0.32$ |
| 269.8 | 1.72 | 1.20 - 2.44 | 2.45 - 9.13 | 5.2 - 9.1 | $5.44 \pm 0.28$ |
| 260.1 | 1.79 | 1.68 - 3.8 | 3.38 - 8.01 | 6.0 - 12 | $5.33 \pm 0.34$ |
| 250.4 | 1.86 | 1.93 - 5.29 | 5.21 - 12.1 | 7.0 - 18 | $5.42 \pm 0.30$ |
| 240.3 | 1.93 | 1.82 - 3.8 | 2.95 - 6.47 | 5.0 - 9.0 | $5.39 \pm 0.46$ |
| 230.3 | 2.02 | 0.75 - 1.90 | 2.43 - 8.46 | 1.8 - 5.2 | $5.99 \pm 0.42$ |

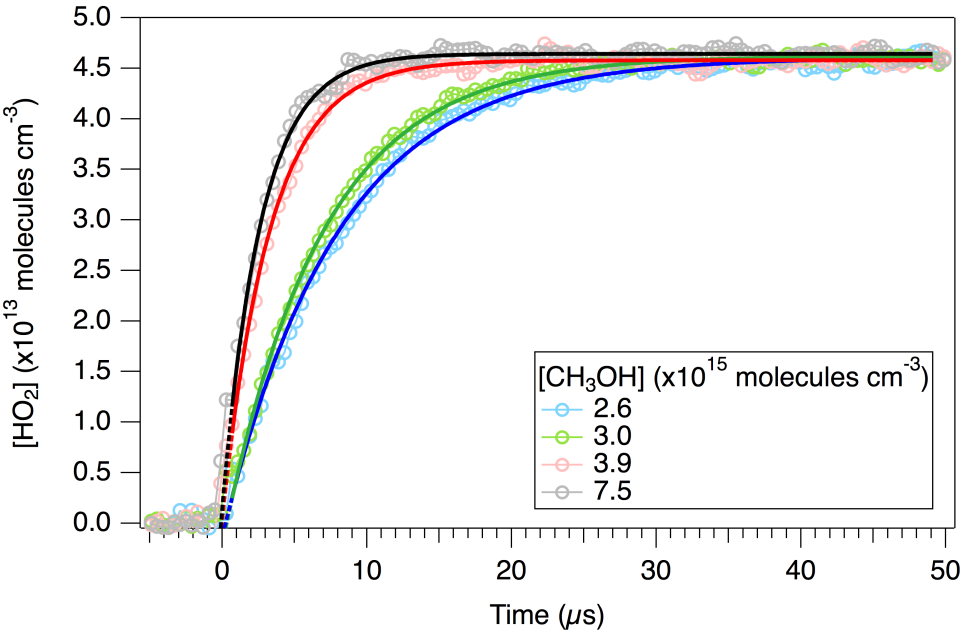


(a)

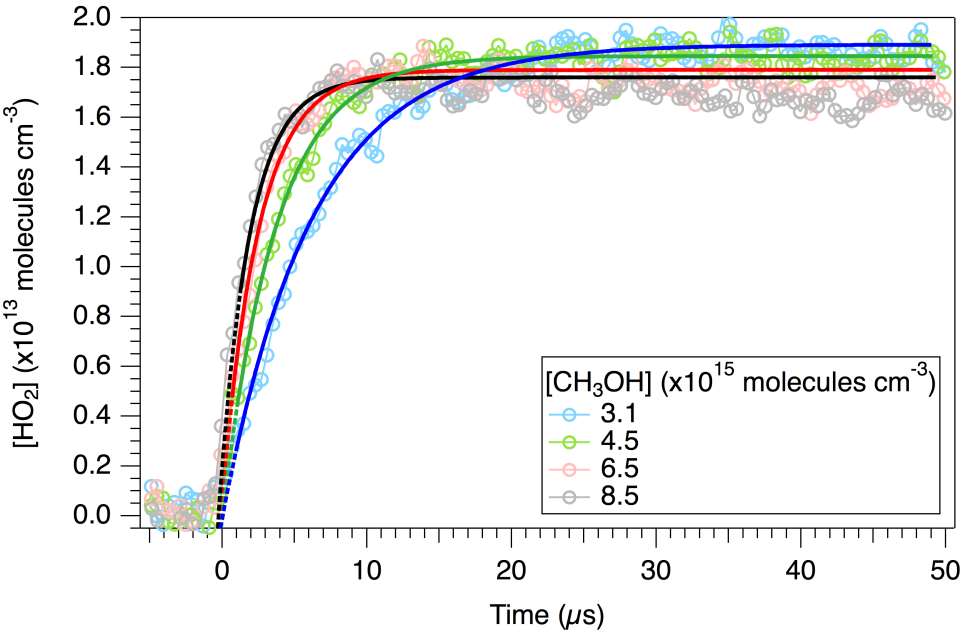


(b)

Figure 1: Example data demonstrating pseudo-first order growths of $HO_2$ using varying [$CH_3OH$] with [$CH_3CHO$] = 0 at (a) $T$ = 294.8 K, $[Cl]_0 = 4.6 \times 10^{13}$ molecules cm$^{-3}$, and (b) $T$ = 230.3 K, $[Cl]_0 = 1.8 \times 10^{13}$ molecules cm$^{-3}$. Dashed lines are the fits extrapolated to $t = 0$.

The Arrhenius expression was found to be $k_1(T) = 5.02^{+1.8}_{-1.5} \times 10^{-11} \exp[(20 \pm 88)/T]$ cm$^3$ molecule$^{-1}$ s$^{-1}$. Within experimental uncertainty, the rate constant was temperature-

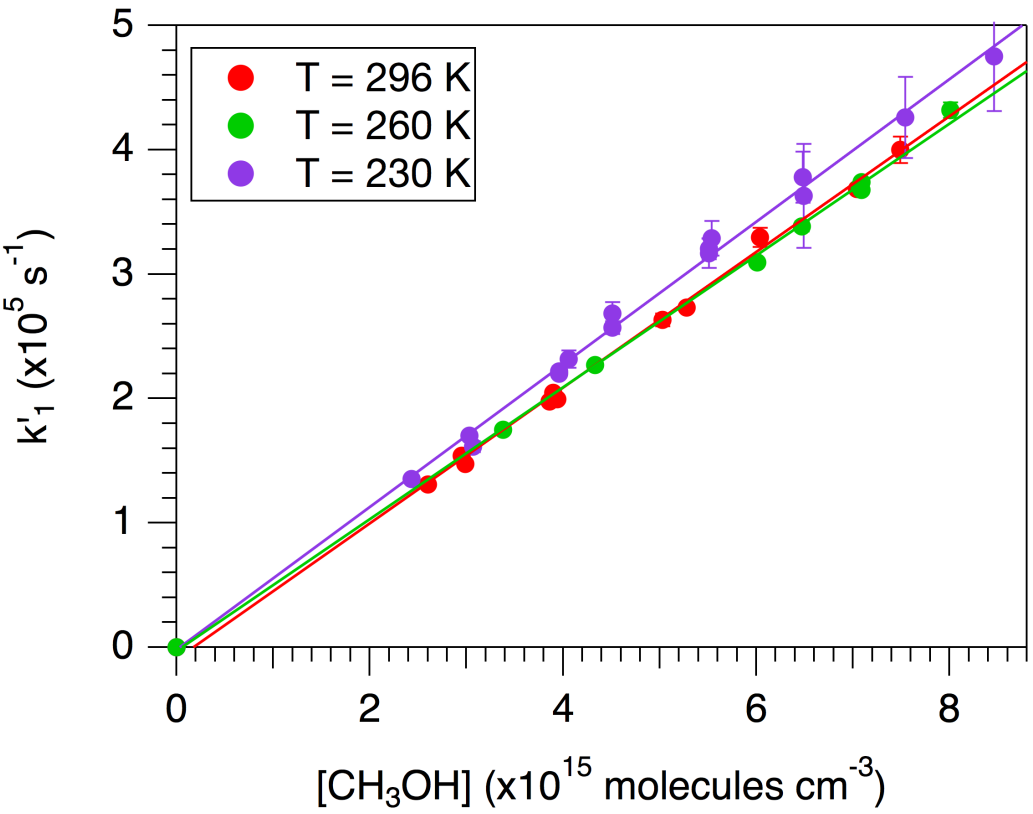


Figure 2: Plot of $k_1$ as a function of $CH_3OH$ at $T$ = 230.3 K, 260.1 K, and 297.1 K.

independent over the temperature range 230.3 - 297.1 K, which is consistent with the results from Michael et al.[38] and Lightfoot et al.[39]. An average value of $k_1 = (5.45 \pm 0.37) \times 10^{-11}$ cm$^3$ molecule$^{-1}$ s$^{-1}$ ($2\sigma$ uncertainty) was determined from the values measured at each temperature weighted by the corresponding uncertainties. Table 2 compares the results from this work with those of previous works in the literature. The results are in excellent agreement with the room temperature values from previous measurements and with the JPL and IUPAC recommendations. $k_1$ was observed to lack a significant temperature dependence, further challenging the previous results by Garzón et al.[40]. Kaiser and Wallington[41] reported a weak temperature dependence for temperatures at and above room temperature, which is beyond the range of temperatures that were studied in this work. Nonetheless, extrapolation of the data from Kaiser and Wallington[41] to lower temperatures results in values that are smaller than our measured values of $k_1$.

**Table 2: Comparison of measured $k_1$ with literature values**

| Ref | T (K) | P (Torr) | $k_1$[a] ($\times 10^{-11}$ cm$^3$ s$^{-1}$) | Method[b] |
|---|---|---|---|---|
| Michael et al.[38] | 200 - 500 | 760 | $6.33 \pm 1.40$ | FP/RF |
| Payne et al.[25] | 298 | 1 | $5.1 \pm 1.0$ | DF/MS |
| Wallington et al.[26] | 295 | 760 | $4.57 \pm 0.40$ | RR/UVP/GC[c] |
| Lightfoot et al.[39] | 248 - 573 | 210 - 760 | $5.3 \pm 2.4$ | RR/FP/UVA[d] |
| Nelson et al.[27] | 298 | 730 - 750 | $4.79 \pm 0.36$ | RR/UVP/GC[e] |
| Dóbé et al.[28] | 298 | 1.35 | $6.14 \pm 1.33$ | DF/EPR |
| Tyndall et al.[29] | 295 | 700 | $5.1 \pm 0.4$ | PLP/RF |
| | | | $5.6 \pm 0.6$ | RR/PLP/RF[c,f] |
| Smith et al.[30] | 295 | 10 | $5.6 \pm 0.2$ | PLP/IR |
| Seakins et al.[31] | 298 | 25 | $5.83 \pm 0.77$ | PLP/IR |
| | | | $5.38 \pm 0.25$ | PLP/CL |
| Taketani et al.[32] | 295 | 3 | $5.35 \pm 0.24$ | PLP/LIF |
| Garzón et al.[40] | 264 - 382 | 20 - 200 | $(35.5 \pm 2.2)\exp[-(559 \pm 40)/T]$ | PLP/RF |
| Kaiser and Wallington[41] | 291 - 475 | 500 - 950 | $8.6 \pm 1.3\exp[-(167 \pm 60)/T]$ | RR/UVP/GC[c] |
| This work | 230.3 - 297.1 | 100 | $5.45 \pm 0.37$ | PLP/IR |
| JPL[42] | 200 - 573 | | 5.5[g] | |
| IUPAC[43] | 200 - 500 | | $7.1\exp(-75/T)$[h] | |

[a] Errors are $2\sigma$
[b] FP = flash photolysis; DF = discharge flow; PLP = pulsed laser photolysis; UVP = UV photolysis; MS = mass spectrometry; GC = gas chromatography; UVA = UV absorption; EPR = electron paramagnetic resonance; RF = resonance fluorescence; IR = IR absorption; CL = chemical luminescence; LIF = laser-induced fluorescence; FTIR = Fourier transform IR spectroscopy; RR= relative rate.
[c] Reference reaction: Cl + $C_2H_6$; $k_{ref} = 5.7 \times 10^{-11}$ cm$^3$ molecule$^{-1}$ s$^{-1}$
[d] Cl + $CH_4$; $k_{ref} = 1.0 \times 10^{-13}$ cm$^3$ molecule$^{-1}$ s$^{-1}$
[e] Cl + $c$–$C_6H_{12}$; $k_{ref} = 3.11 \times 10^{-10}$ cm$^3$ molecule$^{-1}$ s$^{-1}$
[f] Reference reaction: Cl + $C_2H_4$; $k_{ref} = 9.3 \times 10^{-11}$ cm$^3$ molecule$^{-1}$ s$^{-1}$
[g] $\Delta \log_{10} k(298\text{ K}) = 1.2$, $\Delta(E/R) = \pm 100$ K
[h] $\Delta \log_{10} k(298\text{ K}) = 0.07$, $\Delta(E/R) = \pm 200$ K

The uncertainty in the average value of $k_1$ is the weighted standard deviation and includes both random errors in the fits and systematic errors in the measured concentrations of [$CH_3OH$]; systematic errors from secondary chemistry are not included. Under the conditions of these experiments, loss of $HO_2$ from R7 is estimated to be less than 5% across all temperatures, contributing to less than 10% error in the fitted values of $k_1'$. For temperatures below 250 K, the loss of $HO_2$ via R11 becomes more significant; at $T$ = 230.3 K, this is estimated to introduce between 1% to 30% error to $k_1'$ at the lowest and largest [$CH_3OH$].

## Rate constant of Cl + $CH_3CHO$ ($k_3$)

In the presence of $CH_3CHO$, a fraction of the Cl radicals is lost via R3, and the integrated rate law for $HO_2$ is given by Equation 12:

$$[HO_2] = \left(\frac{k_1'}{k_{eff}}\right)[Cl]_0(1 - e^{-k_{eff}t}) \quad (12)$$

where

$$k_{eff} = k_1' + k_3' \quad (13)$$

$k_3'$ was measured at each temperature for varying concentrations of $CH_3OH$ and $CH_3CHO$. Example traces of $HO_2$ in the presence of both $CH_3OH$ and $CH_3CHO$ at two different temperatures are shown in Figure 3. For each temperature, the $HO_2$ profile obtained in the absence of $CH_3CHO$ is provided for reference. In Figure 3(a) and 3(b), the $HO_2$ traces do not level off to a common value due to the additional loss of Cl via R6. Each $HO_2$ time profile was fit to Equation 12, allowing the pre-exponential factor, $A = k_1'[Cl]_0/k_{eff}$, and $k_{eff}$ in the exponent to be varied parameters. The long-time $HO_2$ level (i.e., $t \sim$25 - 50 $\mu$s), which is defined by the pre-exponential factor, $A$, could also be used to estimate $k_{eff}$ without fitting the data with Equation 12. These estimates of $k_{eff}$ were found to be self-consistent with the values of $k_{eff}$ obtained from the fit.

For data sets where [$CH_3CHO$] was varied for a fixed [$CH_3OH$], it was confirmed that the intercept of the linear fit to $k_{eff}$ vs [$CH_3CHO$] yielded $k_1$[$CH_3OH$], where $k_1$ was consistent, within experimental uncertainty, with the measured value of $5.45 \times 10^{-11}$ cm$^3$ molecule$^{-1}$ s$^{-1}$ (Table 2). From Equation 13, $k_3'$ was calculated using the value of $k_1$ determined in this work. Figure 4 shows a plot of $k_3'$ versus [$CH_3CHO$] for three different temperatures. Data from all other temperatures were revealed to have similar linear dependences and have been excluded in the figure for clarity. Values of $k_3$ at each temperature were determined from the slopes of the linear fits to the data.

The average value of $k_3$ determined at each temperature and the range of precursor and

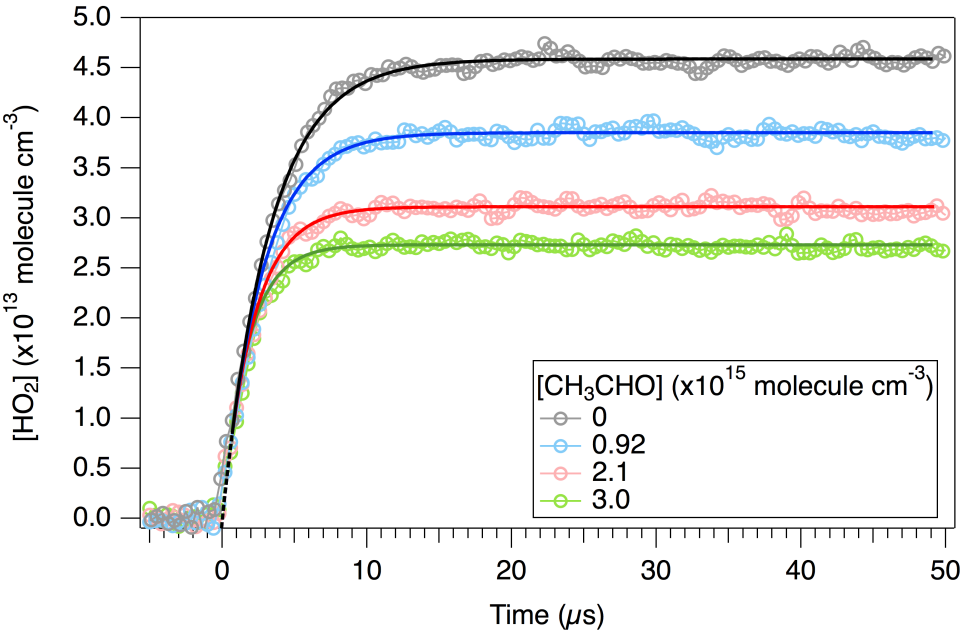


(a)

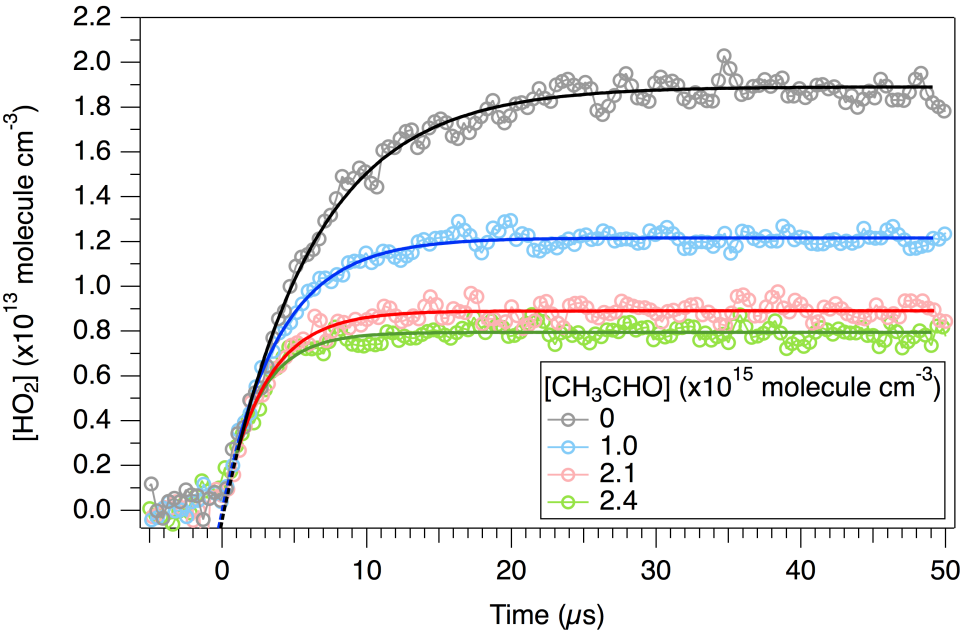


(b)

Figure 3: Example data demonstrating pseudo-first order growths of $HO_2$ using varying [$CH_3CHO$] with fixed [$CH_3OH$] at (a) $T$ = 294.8 K, $[Cl]_0 = 4.6 \times 10^{13}$ molecules cm$^{-3}$, [$CH_3OH$] = $6.1 \times 10^{15}$ molecules cm$^{-3}$, and (b) $T$ = 230.3 K, $[Cl]_0 = 1.8 \times 10^{13}$ molecules cm$^{-3}$, [$CH_3OH$] = $3.1 \times 10^{13}$ molecules cm$^{-3}$. Dashed lines are the fits extrapolated to $t$ = 0.

initial radical concentrations that were used are summarized in Table 3. The uncertainties in $k_3$ ($2\sigma$) include the random errors in $k_3'$ (typical: ~2 - 3%, maximum: ~10%) as well as

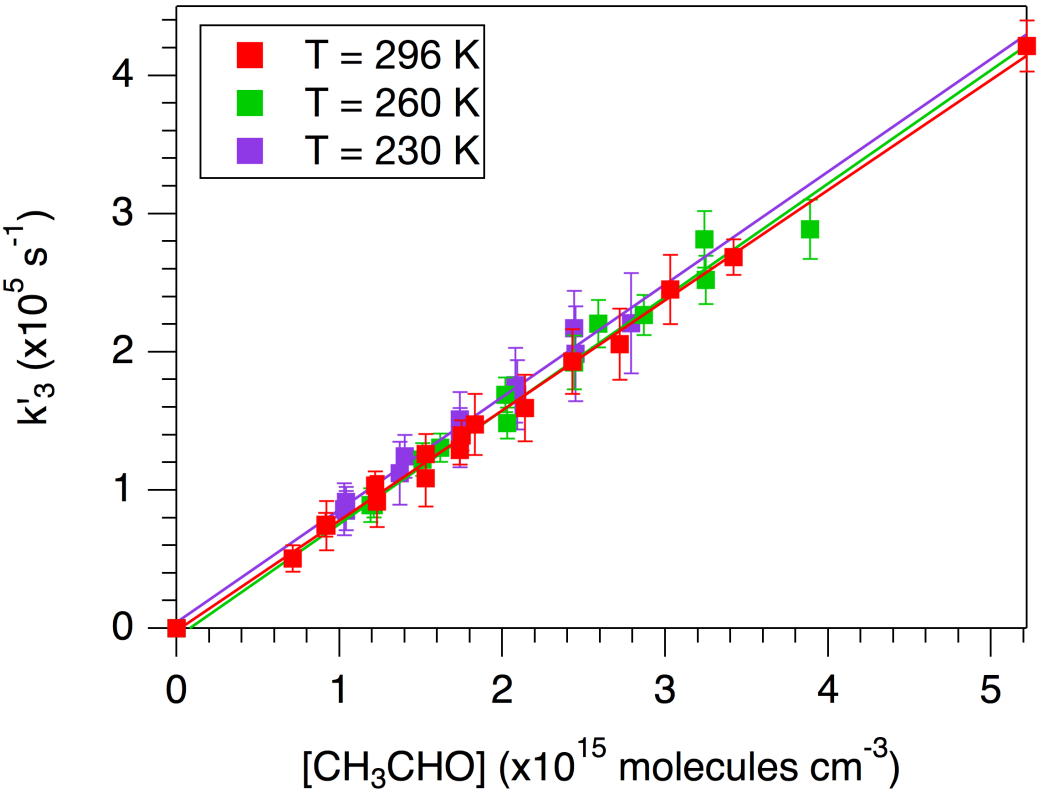


Figure 4: Plot of $k_3$ as a function of $CH_3CHO$ at $T$ = 230 K, 260 K, and 297 K shown with linear fits. All other temperatures have been excluded for clarity. Total linear regression

systematic errors in $k_{eff}$ and in the pressures, flows, and temperatures (total uncertainty in $[CH_3CHO]$: ∼5%).

**Table 3: Experimental conditions for determination of $k_3$. Uncertainties in $k_3$ are $2\sigma$.**

| T (K) | $[O_2]$ ($\times 10^{18}$ cm$^{-3}$) | $[Cl_2]$ ($\times 10^{15}$ cm$^{-3}$) | $[CH_3OH]$ ($\times 10^{15}$ cm$^{-3}$) | $[CH_3CHO]$ ($\times 10^{15}$ cm$^{-3}$) | $[CH_3OH]/[CH_3CHO]$ | $[Cl]_0$ ($\times 10^{13}$ cm$^{-3}$) | $k_3$ ($\times 10^{-11}$ cm$^3$ s$^{-1}$) |
|---|---|---|---|---|---|---|---|
| 297.1 | 1.58 | 3.02 - 5.29 | 3.90 | 0.71 - 5.22 | 2.25 - 6.60 | 19 | $8.16 \pm 1.08$ |
| 294.8 | 1.58 | 1.49 | 3.00 - 6.08 | 0.92 - 3.03 | 0.75 - 5.46 | 4.5 | $7.61 \pm 1.78$ |
| 280.2 | 1.66 | 1.56 | 2.97 - 4.99 | 0.95 - 1.93 | 1.87 - 6.80 | 5.1 - 13 | $7.24 \pm 2.34$ |
| 269.8 | 1.72 | 1.61 - 2.12 | 4.01 - 6.06 | 0.97 - 5.11 | 0.97 - 5.14 | 5.3 - 7.5 | $7.78 \pm 1.00$ |
| 260.1 | 1.79 | 1.68 | 3.44 - 4.40 | 1.19 - 3.89 | 1.12 - 3.73 | 6.0 | $8.21 \pm 1.26$ |
| 250.4 | 1.86 | 1.93 - 3.53 | 5.23 - 6.35 | 1.26 - 8.43 | 0.62 - 4.14 | 7.1 - 1.2 | $8.11 \pm 0.74$ |
| 240.3 | 1.93 | 1.82 | 2.96 - 5.98 | 0.98 - 4.56 | 1.31 - 6.10 | 5.0 | $7.95 \pm 1.22$ |
| 230.3 | 2.02 | 0.75 | 3.08 - 5.10 | 1.03 - 2.80 | 1.45 - 4.93 | 1.8 | $8.16 \pm 2.36$ |

The Arrhenius expression was found to be $k_3(T) = 6.38^{+2.4}_{-2.0} \times 10^{-11} \exp[(56 \pm 90)/T]$ cm$^3$ molecule$^{-1}$ s$^{-1}$. Similarly to R1, R3 was revealed to have no discernible temperature dependence in the temperature range $T$ = 230.3 - 297.1 K, with an average value of $k_3 =$

$(8.00 \pm 1.27) \times 10^{-11}$ cm$^3$ molecule$^{-1}$ s$^{-1}$ ($2\sigma$ uncertainty). The uncertainty is the weighted standard deviation and includes both systematic and random errors. This is in excellent agreement with previous measurements and with the IUPAC recommendation (Table 4). Our conclusion that $k_3$ has no significant temperature dependence over our experimental temperature range is consistent with the only previous temperature-dependence study by Payne et al.[44]. Although our value of $k_3$ is higher than that reported by Payne et al.[44], our results are still within their $2\sigma$ uncertainty bounds.

As mentioned in previous works by Michael et al.[38] and Payne et al.[44], the temperature dependence of hydrogen abstraction reactions of related oxygenated hydrocarbons by Cl can be predicted based on the R−H bond energies. Specifically, hydrogen abstraction reactions by Cl for R−H molecules with bond energies between those of $C_2H_6$ (98 kcal/mol) and $CH_2O$ (86 kcal/mol) are expected to be temperature-independent, based on the observation that $C_2H_6$ and $CH_2O$ were respectively found to have minimal to no temperature dependence in their reactions with Cl. The bond energies for the C−H bond in $CH_3OH$ and in the aldehydic C−H bond in $CH_3CHO$ are both ∼95 kcal/mol.[53–55] Based on the empirical correlation between the R−H bond energies and the observed temperature dependence of the Cl reactions, R1 and R3 are expected to show no temperature dependence, which is consistent with our results.

# Conclusion

The absolute rate constants of the reactions of Cl atoms with $CH_3OH$ and $CH_3CHO$ have been determined at 100 Torr over the temperature range 230.3 K - 297.1 K by measuring the formation rate of $HO_2$ in various relative concentrations of $CH_3OH$ and $CH_3CHO$. The values of the rate constants at room temperature are in excellent agreement with previous measurements and support the current recommendations by the JPL and IUPAC evaluations.

**Table 4: Comparison of measured $k_3$ with literature values**

| Ref | T (K) | P (Torr) | $k_3$[a] ($\times 10^{-11}$ cm$^3$ s$^{-1}$) | Method[b] |
|---|---|---|---|---|
| Niki et al.[33] | 298 | 700 | $7.6 \pm 0.4$ | RR/UVP/FTIR[c] |
| Wallington et al.[26] | 295 | 760 | $8.45 \pm 0.79$ | RR/UVP/GC[c] |
| Bartels et al.[34] | 298 | 0.75 | $6.0 \pm 0.9$ | RR/DF/MS[c] |
| Payne et al.[44] | 210 - 343 | 25 - 200 | $6.6 \pm 1.4$ | FP/RF |
| Scollard et al.[35] | 298 | 730 - 750 | $7.9 \pm 0.6$ | RR/UVP/GC[d] |
| Tyndall et al.[29] | 295 | 700 | $7.3 \pm 0.7$ | PLP/RF |
| | | | $8.4 \pm 1.0$ | RR/PLP/RF[c,e] |
| Kegley-Owen et al.[36] | 298 | 10 - 50 | $7.5 \pm 0.8$ | PLP/IR |
| Smith et al.[30] | 295 | 10 | $8.3 \pm 0.1$ | PLP/IR |
| Seakins et al.[31] | 298 | 25 | $7.7 \pm 1.1$ | PLP/IR |
| | 298 | | $8.8 \pm 1.5$ | PLP/CL |
| Howes et al.[37] | 298 | 1-2 | $7.7 \pm 0.7$ | PLP/MS |
| This work | 230.3 - 297.1 | 100 | $8.00 \pm 1.27$ | PLP/IR |
| IUPAC[43] | 210 - 340 | | 8.0[f] | |

[a] Errors are $2\sigma$
[b] FP = flash photolysis; PLP = pulsed laser photolysis; UV = UV photolysis; RF = resonance fluorescence; IR = IR absorption; CL = CL chemical luminescence; FTIR = Fourier transform IR spectroscopy; GC = gas chromatography; MS = mass spectrometry; RR= relative rate.
[c] Reference reaction: Cl + $C_2H_6$; $k_{ref} = 5.7 \times 10^{-11}$ cm$^3$ molecule$^{-1}$ s$^{-1}$
[d] Reference reaction: Cl + $(CH_3)_2O$; $k_{ref} = 1.76 \times 10^{-10}$ cm$^3$ molecule$^{-1}$ s$^{-1}$
[e] Reference reaction: Cl + $C_2H_4$; $k_{ref} = 9.3 \times 10^{-11}$ cm$^3$ molecule$^{-1}$ s$^{-1}$
[f] $\Delta \log_{10} k(298\ \mathrm{K}) = 0.07$, $\Delta(E/R) = \pm 200$ K

Both $k_1$ and $k_3$ were found to be temperature independent over our temperature range, within experimental uncertainty. The lack of a temperature dependence for $k_1$ is consistent with the previous work by Michael et al.[38] and Lightfoot et al.[39] and challenges the results from Garzón et al.[40]. Extrapolation of the results from Kaiser and Wallington[41] to lower temperatures underestimate our measured values of $k_1$; however, additional experiments that cover temperatures both below and above room temperature are needed for further assessment. The temperature independence of $k_3$ validate the results from the only temperature dependence of R3 by Payne et al.[44]. Our value of $k_3$ was higher than that reported by Payne et al.[44], but was still within experimental error.

The results from this work provide experimental data for $k_1$ and $k_3$ over a temperature range that is relevant for the Earth's lower atmosphere. Although R1 and R3 are unlikely to play key roles in the atmosphere directly, they are both commonly used to generate

peroxy radicals in the laboratory for studying other reactions that are important in the troposphere. Therefore, well-defined values for $k_1$ and $k_3$ enable accurate characterization of peroxy radical reactions over a wide range of atmospherically-relevant temperatures.

## Acknowledgement

This research was carried out by the Jet Propulsion Laboratory, California Institute of Technology, under contract with the National Aeronautics and Space Administration (NASA). The authors thank the National Science Foundation (NSF Grant No. CHE-1413712), the NASA Earth and Space Science Fellowship (NESSF), and NASA's Upper Atmospheric Research Program (UARP Grant No. NNX12AE01G) and Tropospheric Chemistry Program for financial support. 

## Supporting Information Available

Comparison of fitted values of $k_1$ and $k_3$ using pseudo-first order approximation and using kinetics model with second-order $HO_2$ loss; complete list of experimental conditions used for the determination of $k_1$ and $k_3$.

## References

(1) Spicer, C. W.; Chapman, E. G.; Finlayson-Pitts, B. J.; Plastridge, R. A.; Hubbe, J. M.; Fast, J. D.; Berkowitz, C. M. Unexpectedly High Concentrations of Molecular Chlorine in Coastal Air. *Nature* **1998**, *394*, 353.

(2) Keene, W. C.; Stutz, J.; Pszenny, A. A. P.; Maben, J. R.; Fischer, E. V.; Smith, A. M.; von Glasow, R.; Pechtl, S.; Sive, B. C.; Varner, R. K. Inorganic Chlorine and Bromine in Coastal New England Air during Summer. *J. Geophys. Res.-Atmos* **2007**, *112*.

(3) Finley, B. D.; Saltzman, E. S. Observations of $Cl_2$, $Br_2$, and $I_2$ in Coastal Marine Air. *J. Geophys. Res.-Atmos* **2008**, *113*.

(4) Ravishankara, A. R. Are Chlorine Atoms Significant Tropospheric Free Radicals? *PNAS* **2009**, *106*, 13639–13640.

(5) Kercher, J. P.; Riedel, T. P.; Thornton, J. A. Chlorine Activation by $N_2O_5$: Simultaneous, in Situ Detection of $ClNO_2$ and $N_2O_5$ by Chemical Ionization Mass Spectrometry. *Atmos. Meas. Tech.* **2009**, *2*, 193–204.

(6) Roberts, J. M.; Osthoff, H. D.; Brown, S. S.; Ravishankara, A. R. $N_2O_5$ Oxidizes Chloride to $Cl_2$ in Acidic Atmospheric Aerosol. *Science* **2008**, *321*, 1059–1059.

(7) Osthoff, H. D.; Roberts, J. M.; Ravishankara, A. R.; Williams, E. J.; Lerner, B. M.; Sommariva, R.; Bates, T. S.; Coffman, D.; Quinn, P. K.; Dibb, J. E. et al. High Levels of Nitryl Chloride in the Polluted Subtropical Marine Boundary Layer. *Nat. Geosci.* **2008**, *1*, 324–328.

(8) Behnke, W.; George, C.; Scheer, V.; Zetzsch, C. Production and Decay of $ClNO_2$ from the Reaction of Gaseous $N_2O_5$ with NaCl Solution: Bulk and Aerosol Experiments. *J. Geophys. Res.-Atmos* **1997**, *102*, 3795–3804.

(9) Finlayson-Pitts, B. J.; Ezell, M. J.; Pitts, J. N. Formation of Chemically Active Chlorine Compounds by Reactions of Atmospheric NaCl Particles with Gaseous $N_2O_5$ and $ClONO_2$. *Nature* **1989**, *337*, 241.

(10) Raff, J. D.; Njegic, B.; Chang, W. L.; Gordon, M. S.; Dabdub, D.; Gerber, R. B.; Finlayson-Pitts, B. J. Chlorine Activation Indoors and Outdoors via Surface-Mediated Reactions of Nitrogen Oxides with Hydrogen Chloride. *Proc. Natl. Acad. Sci. U.S.A.* **2009**, *106*, 13647–13654.

(11) Jacob, D. J.; Field, B. D.; Li, Q.; Blake, D. R.; de Gouw, J.; Warneke, C.; Hansel, A.; Wisthaler, A.; Singh, H. B.; Guenther, A. Global Budget of Methanol: Constraints from Atmospheric Observations. *J. Geophys. Res.-Atmos* **2005**, *110*.

(12) Millet, D. B.; Apel, E.; Henze, D. K.; Hill, J.; Marshall, J. D.; Singh, H. B.; Tessum, C. W. Natural and Anthropogenic Ethanol Sources in North America and Potential Atmospheric Impacts of Ethanol Fuel Use. *Environ. Sci. Technol.* **2012**, *46*, 8484–8492.

(13) Luecken, D.; Hutzell, W.; Strum, M.; Pouliot, G. Regional Sources of Atmospheric Formaldehyde and Acetaldehyde, and Implications for Atmospheric Modeling. *Atmos. Environ.* **2012**, *47*, 477–490.

(14) Atkinson, R. Gas-Phase Tropospheric Chemistry of Volatile Organic Compounds: 1. Alkanes and Alkenes. *J. Phys. Chem. Ref. Data* **1997**, *26*, 215–290.

(15) Hui, A. O.; Fradet, M.; Okumura, M.; Sander, S. P. Temperature Dependence Study of the Kinetics and Product Yields of the $HO_2$ + $CH_3C(O)O_2$ Reaction by Direct Detection of OH and $HO_2$ Radicals Using 2f-IR Wavelength Modulation Spectroscopy. *J. Phys. Chem. A* **2019**, *0*, null.

(16) Moortgat, G.; Veyret, B.; Lesclaux, R. Absorption Spectrum and Kinetics of Reactions of the Acetylperoxy Radical. *J. Phys. Chem.* **1989**, *93*, 2362 – 2368.

(17) Crawford, M. A.; Wallington, T. J.; Szente, J. J.; Maricq, M. M.; Francisco, J. S. Kinetics and Mechanism of the Acetylperoxy + $HO_2$ Reaction. *J. Phys. Chem. A* **1999**, *103*, 365–378.

(18) Tomas, A.; Villenave, E.; Lesclaux, R. Reactions of the $HO_2$ Radical with $CH_3CHO$ and $CH_3C(O)O_2$ in the Gas Phase. *J. Phys. Chem. A* **2001**, *105*, 3505–3514.

(19) Hasson, A. S.; Tyndall, G. S.; Orlando, J. J. A Product Yield Study of the Reaction of

$HO_2$ Radicals with Ethyl Peroxy ($C_2H_5O_2$), Acetyl Peroxy ($CH_3C(O)O_2$), and Acetonyl Peroxy ($CH_3C(O)CH_2O_2$) Radicals. *J. Phys. Chem. A* **2004**, *108*, 5979–5989.

(20) Le Crâne, J.-P.; Rayez, M.-T.; Rayez, J.-C.; Villenave, E. A Reinvestigation of the Kinetics and the Mechanism of the $CH_3C(O)O_2$ + $HO_2$ Reaction Using Both Experimental and Theoretical Approaches. *Phys. Chem. Chem. Phys.* **2006**, *8*, 2163–2171.

(21) Jenkin, M. E.; Hurley, M. D.; Wallington, T. J. Investigation of the Radical Product Channel of the $CH_3C(O)O_2$ + $HO_2$ Reaction in the Gas Phase. *Phys. Chem. Chem. Phys.* **2007**, *9*, 3149–3162.

(22) Dillon, T. J.; Crowley, J. N. Direct Detection of OH Formation in the Reactions of $HO_2$ with $CH_3C(O)O_2$ and Other Substituted Peroxy Radicals. *Atmospheric Chem. Phys.* **2008**, *8*, 4877–4889.

(23) Groß, C. B. M.; Dillon, T. J.; Schuster, G.; Lelieveld, J.; Crowley, J. N. Direct Kinetic Study of OH and $O_3$ Formation in the Reaction of $CH_3C(O)O_2$ with $HO_2$. *J. Phys. Chem. A* **2014**, *118*, 974–985.

(24) Winiberg, F. A. F.; Dillon, T. J.; Orr, S. C.; Groß, C. B. M.; Bejan, I.; Brumby, C. A.; Evans, M. J.; Smith, S. C.; Heard, D. E.; Seakins, P. W. Direct Measurements of OH and Other Product Yields from the $HO_2$ + $CH_3C(O)O_2$ Reaction. *Atmos. Chem. Phys.* **2016**, *16*, 4023–4042.

(25) Payne, W. A.; Brunning, J.; Mitchell, M. B.; Stief, L. J. Kinetics of the Reactions of Atomic Chlorine with Methanol and the Hydroxymethyl Radical with Molecular Oxygen at 298 K. *Int. J. Chem. Kinet.* **1988**, *20*, 63–74.

(26) Wallington, T. J.; Skewes, L. M.; Siegl, W. O.; Wu, C.-H.; Japar, S. M. Gas Phase Reaction of Cl Atoms with a Series of Oxygenated Organic Species at 295 K. *Int. J. Chem. Kinet.* **1988**, *20*, 867–875.

(27) Nelson, L.; Rattigan, O.; Neavyn, R.; Sidebottom, H.; Treacy, J.; Nielsen, O. J. Absolute and Relative Rate Constants for the Reactions of Hydroxyl Radicals and Chlorine Atoms with a Series of Aliphatic Alcohols and Ethers at 298 K. *Int. J. Chem. Kinet.* **1990**, *22*, 1111–1126.

(28) Dóbé, S.; Otting, M.; Temps, F.; Wagner, H. G.; Ziemer, H. Fast Flow Kinetic Studies of the Reaction $CH_2OH + HCl \leftrightharpoons CH_3OH + Cl$. The Heat of Formation of Hydroxymethyl. *Ber. Bunsen-Ges. Phys. Chem.* **1993**, *97*, 877–883.

(29) Tyndall, G. S.; Orlando, J. J.; Kegley-Owen, C. S.; Wallington, T. J.; Hurley, M. D. Rate Coefficients for the Reactions of Chlorine Atoms with Methanol and Acetaldehyde. *Int. J. Chem. Kinet.* **1999**, *31*, 776–784.

(30) Smith, J. D.; DeSain, J. D.; Taatjes, C. A. Infrared Laser Absorption Measurements of HCl(V=1) Production in Reactions of Cl Atoms with Isobutane, Methanol, Acetaldehyde, and Toluene at 295 K. *Chem. Phys. Lett.* **2002**, *366*, 417–425.

(31) Seakins, P. W.; Orlando, J. J.; Tyndall, G. S. Rate Coefficients and Production of Vibrationally Excited HCl from the Reactions of Chlorine Atoms with Methanol, Ethanol, Acetaldehyde and Formaldehyde. *Phys. Chem. Chem. Phys.* **2004**, *6*, 2224–2229.

(32) Taketani, F.; Takahashi, K.; Matsumi, Y.; Wallington, T. J. Kinetics of the Reactions of $Cl^*(^2P_{1/2})$ and $Cl(^2P_{3/2})$ Atoms with $CH_3OH$, $C_2H_5OH$, n-$C_3H_7OH$, and i-$C_3H_7OH$ at 295 K. *J. Phys. Chem. A* **2005**, *109*, 3935–3940.

(33) Niki, H.; Maker, P. D.; Savage, C. M.; Breitenbach, L. P. FTIR Study of the Kinetics and Mechanism for Chlorine-Atom-Initiated Reactions of Acetaldehyde. *J. Phys. Chem.* **1985**, *89*, 588–591.

(34) Bartels, M.; Hoyermann, K.; Lange, U. An Experimental Study of the Reactions

$CH_3CHO$ + Cl, $C_2H_4O$ + Cl, and $C_2H_4O$ + F in the Gas-Phase. *Ber. Bunsen-Ges. Phys. Chem.* **1989**, *93*, 423–427.

(35) Scollard, D. J.; Treacy, J. J.; Sidebottom, H. W.; Balestra-Garcia, C.; Laverdet, G.; LeBras, G.; MacLeod, H.; Teton, S. Rate Constants for the Reactions of Hydroxyl Radicals and Chlorine Atoms with Halogenated Aldehydes. *J. Phys. Chem.* **1993**, *97*, 4683–4688.

(36) Kegley-Owen, C. S.; Tyndall, G. S.; Orlando, J. J.; Fried, A. Tunable Diode Laser Studies of the Reaction of Cl Atoms with $CH_3CHO$. *Int. J. Chem. Kinet.* **1999**, *31*, 766–775.

(37) Howes, N. U. M.; Lockhart, J. P. A.; Blitz, M. A.; Carr, S. A.; Baeza-Romero, M. T.; Heard, D. E.; Shannon, R. J.; Seakins, P. W.; Varga, T. Observation of a New Channel, the Production of $CH_3$, in the Abstraction Reaction of OH Radicals with Acetaldehyde. *Phys. Chem. Chem. Phys.* **2016**, *18*, 26423–26433.

(38) Michael, J. V.; Nava, D. F.; Payne, W. A.; Stiefb), L. J. Rate Constants for the Reaction of Atomic Chlorine with Methanol and Dimethyl Ether from 200 to 500 K. *J. Chem. Phys.* **1979**, *70*, 3652–3656.

(39) Lightfoot, P. D.; Veyret, B.; Lesclaux, R. Flash Photolysis Study of the Methylperoxy + Hydroperoxy Reaction between 248 and 573 K. *J. Phys. Chem.* **1990**, *94*, 708–714.

(40) Garzón, A.; Cuevas, C. A.; Ceacero, A. A.; Notario, A.; Albaladejo, J.; Fernández-Gómez, M. Atmospheric Reactions Cl+$CH_3$–($CH_2$)n–OH (N=0–4): A Kinetic and Theoretical Study. *J. Chem. Phys.* **2006**, *125*, 104305.

(41) Kaiser, E. W.; Wallington, T. J. Rate Constant of the Reaction of Chlorine Atoms with Methanol over the Temperature Range 291–475 K. *Int. J. Chem. Kinet.* **2010**, *42*, 113–116.

(42) Burkholder, J. B.; Sander, S. P.; Abbatt, J.; Barker, J. R.; Huie, R.; Kolb, C. E.; Kurylo, M.; Orkin, V.; Wilmouth, D.; Wine, P. H. *Chemical Kinetics and Photochemical Data for Use in Atmospheric Studies, Evaluation No. 18*; 2015.

(43) Atkinson, R.; Baulch, D. L.; Cox, R. A.; Hampson, R. F.; Kerr, J. A.; Troe, J. Evaluated Kinetic and Photochemical Data for Atmospheric Chemistry: Supplement IV. IUPAC Subcommittee on Gas Kinetic Data Evaluation for Atmospheric Chemistry. *J. Phys. Chem. Ref. Data* **1992**, *21*, 1125–1568.

(44) Payne, W. A.; Nava, D. F.; Nesbitt, F. L.; Stief, L. J. Rate Constant for the Reaction of Atomic Chlorine with Acetaldehyde from 210 to 343 K. *J. Phys. Chem.* **1990**, *94*, 7190–7193.

(45) Christensen, L. E.; Okumura, M.; Sander, S. P.; Friedl, R. R.; Miller, C. E.; Sloan, J. J. Measurements of the Rate Constant of $HO_2$ + $NO_2$ + $N_2$ $\rightarrow$ $HO_2NO_2$ + $N_2$ Using Near-Infrared Wavelength-Modulation Spectroscopy and UV-Visible Absorption Spectroscopy. *J. Phys. Chem. A* **2004**, *108*, 80–91.

(46) Noell, A. C.; Alconcel, L. S.; Robichaud, D. J.; Okumura, M.; Sander, S. P. Near-Infrared Kinetic Spectroscopy of the $HO_2$ and $C_2H_5O_2$ Self-Reactions and Cross Reactions. *J. Phys. Chem. A* **2010**, *114*, 6983–6995.

(47) Grieman, F. J.; Noell, A. C.; Davis-Van Atta, C.; Okumura, M.; Sander, S. P. Determination of Equilibrium Constants for the Reaction Between Acetone and $HO_2$ Using Infrared Kinetic Spectroscopy. *J. Phys. Chem. A* **2011**, *115*, 10527–10538.

(48) Onel, L.; Brennan, A.; Gianella, M.; Ronnie, G.; Lawry Aguila, A.; Hancock, G.; Whalley, L.; Seakins, P. W.; Ritchie, G. A. D.; Heard, D. E. An Intercomparison of $HO_2$ Measurements by Fluorescence Assay by Gas Expansion and Cavity Ring-down Spectroscopy within HIRAC (Highly Instrumented Reactor for Atmospheric Chemistry). *Atmos. Meas. Tech.* **2017**, *10*, 4877–4894.

(49) FACSIMILE. MCPA Software Ltd, 2003.

(50) Atkinson, R.; Baulch, D. L.; Cox, R. A.; Crowley, J. N.; Hampson, R. F.; Hynes, R. G.; Jenkin, M. E.; Rossi, M. J.; Troe, J.; IUPAC Subcommittee, Evaluated Kinetic and Photochemical Data for Atmospheric Chemistry: Volume II – Gas Phase Reactions of Organic Species. *Atmos. Chem. Phys.* **2006**, *6*, 3625–4055.

(51) Christensen, L. E.; Okumura, M.; Hansen, J. C.; Sander, S. P.; Francisco, J. S. Experimental and Ab Initio Study of the $HO_2 \cdot CH_3OH$ Complex: Thermodynamics and Kinetics of Formation. *J. Phys. Chem. A* **2006**, *110*, 6948–6959.

(52) Hui, A. O. Atmospheric Peroxy Radical Chemistry Studied by Infrared Kinetic Spectroscopy. Ph.D., California Institute of Technology, Pasadena, CA, 2019.

(53) Cruickshank, F. R.; Benson, S. W. Carbon-Hydrogen Bond Dissociation Energy in Methanol. *J. Phys. Chem.* **1969**, *73*, 733–737.

(54) Lee, J.; Bozzelli, J. W. Reaction of H + Ketene to Formyl Methyl and Acetyl Radicals and Reverse Dissociations. *Int. J. Chem. Kinet.* **2003**, *35*, 20–44.

(55) da Silva, G.; Bozzelli, J. W. Enthalpies of Formation, Bond Dissociation Energies, and Molecular Structures of the n-Aldehydes (Acetaldehyde, Propanal, Butanal, Pentanal, Hexanal, and Heptanal) and Their Radicals. *J. Phys. Chem. A* **2006**, *110*, 13058–13067.

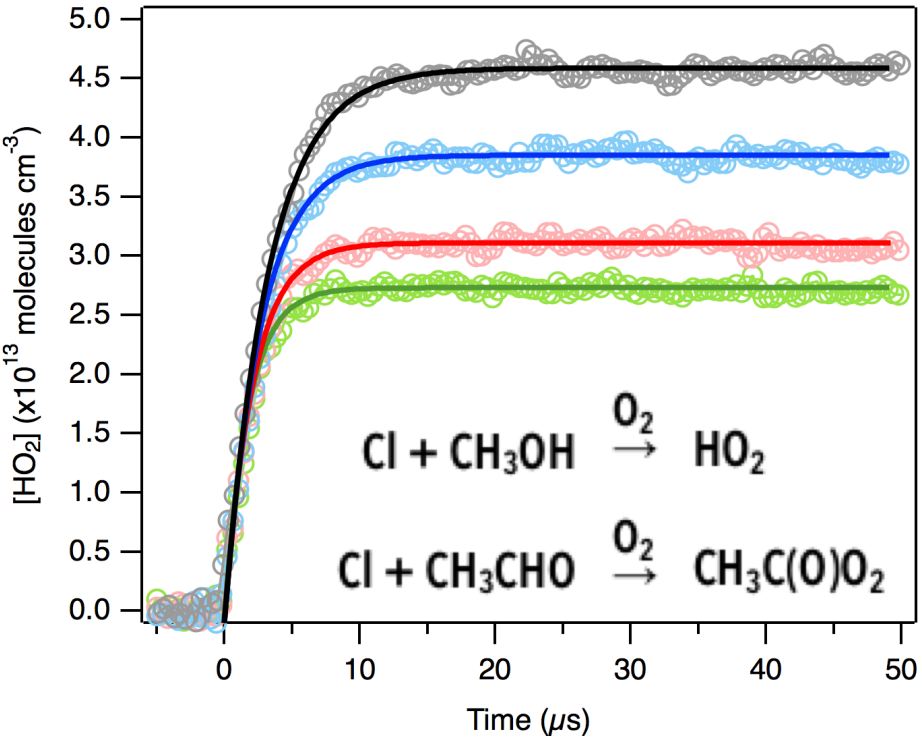


Figure 5: TOC Graphic